Journal of Applied Polymer Science

POSS-based molecular hybrids with low dielectric constant: Effect of chemical structure and molecular architecture

Fuyou Ke, Chao Zhang, Shanyi Guang, Hongyao Xu, Naibo Lin
College of Material Science and Engineering and State Key Laboratory for Modification of Chemical Fibers and Polymer Materials, Donghua University, Shanghai 201620, China
Correspondence to: H. Xu (E-mail: hongyaoxu@163.com)

ABSTRACT: Three kinds of hybrids with different architectures including dumbbell-type, bead-type, and cross-linked structure, were prepared via the Heck reaction between octavinyl-polyhedral oligomeric silsesquioxane (OV-POSS) and different bromo-substituted aromatic amide monomers. The molecular architecture can be successfully achieved by simply varying the feed ratio of OV-POSS to monomers. Their structure and properties were characterized by FTIR, ^{1}H NMR, ^{29}Si NMR, provide the expansion for FTIR and NMR] All the POSS-based hybrids exhibited good thermal stability and low dielectric constant properties. The relationship between chemical structure, molecular architecture, and the dielectric constant of these hybrids were investigated in detail. The results show that POSS content dominated the low dielectric constant of the hybrids, while the chemical structure of organic chains and molecular architecture also play an important role on the formation of low dielectric constant. © 2015 Wiley Periodicals, Inc. J. Appl. Polym. Sci. **2015**, *132*, 42292.

KEYWORDS: composites; dielectric properties; films

Received 26 December 2014; accepted 31 March 2015
DOI: 10.1002/app.42292

INTRODUCTION

Organic-inorganic hybrids have attracted much attention recently due to their advantageous materials performance compared to the nonhybrid counterparts. In particular, the molecular hybrids based on polyhedral oligomeric silsesquioxanes (POSS) that has well defined nanometer-sized cube-like structures with porous inorganic core surrounded by eight organic corner groups (active or inert), can effectively overcome the difficulty to disperse the particles into organic/polymer matrix uniformly via covalent bonding.[1] As a result, the incorporation of POSS has led to enhancement in the physical properties of materials such as thermal and mechanical stability,[2–4] flammability,[5,6] oxidative resistance,[7] and low dielectric constant.[8–10] Thus POSS-based hybrids have been widely studied in many areas of potential use, such as luminescence emission,[11–13] nonlinear optics,[14,15] resist coatings for lithography,[1] laser protection,[16] integrated circuits industry as low dielectric constant materials,[17,18] and so on.[19]

To overcome signal delays and crosstalk noise between the metal interconnects within integrated circuits, low dielectric constant materials are urgently demanded to satisfy the rapid development of microelectronics industry. Owing to its intrinsic porosity, it has been demonstrated that polyimide materials with POSS moieties as chain ends,[20] core in star polymers,[21] pendant groups for the main chains and grafted side chains,[22–25] or even in the main chains[26,27] and network[28–30] exhibited lower dielectric constant than the host polymers, and the dielectric constant can be tuned by adjusting the POSS content. As the POSS content increases, the dielectric constant decreases. Besides construction of different molecular architectures, several fabrication methods were also used to improve the performance of low dielectric constant materials, including chemical vapor deposition,[31] spinning coating,[32] calcinations at high temperature,[33] layer-by-layer assembly,[34,35] and POSS orientation into lamellar structure.[36]

The low dielectric constant of POSS-based hybrids is mainly attributed to the increase of free volume. It is inferred from the previous studies that low dielectric constant depends on the chemical structure of organic chains and molecular architecture. For example, it is well known that adding fluoride into organic chains can reduce the dielectric constant.[37] However, the mechanism of dielectric constant variation related to the chemical structure and molecular architecture has not been fully understood up to now. Recently, our group synthesized a series of network-like hybrids with different flexible organic linking chains between POSS cages via hydrosilylative addition reaction between octahydrido-POSS and diene.[38] These POSS-based hybrid materials exhibited high thermal stability, good mechanical properties, and controllable low dielectric constants by changing the length of organic linking chains. With the methylene number increasing from 2 to 8, the dielectric constants of

© 2015 Wiley Periodicals, Inc.

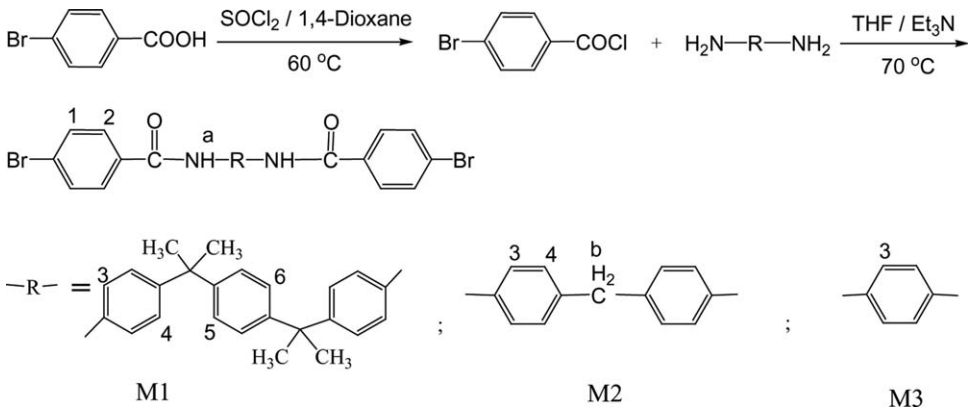

Scheme 1. Synthetic route of the M1~M3.

the hybrid films were reduced from 2.78 to 2.43. After calcination process, the dielectric constant can be further decreased to 1.95.[39]

In our another work, POSS-based hybrids with different molecular architectures including pendent-type and star-type hybrids with flexible organic chains were successfully synthesized and the dependence of the dielectric constant on molecular architecture was investigated in detail.[40] It is showed that star-type POSS-based hybrids exhibit the lower dielectric constants than pendent-type with the same POSS content because of the larger free volume in the hybrids. To further explore the influence of chemical structure and molecular architecture on dielectric constants, in this article, a series of POSS-based molecular hybrids with low dielectric constant, including dumbbell-type, bead-type, and cross-linked network with rigid organic linked chains were prepared (Schemes 1 and 2). The relationships between chemical structure, molecular architecture, and the low dielectric constant, as well as their roles on the formation of low dielectric constant were investigated in detail.

EXPERIMENTAL

Materials

1,4-Benzenediamine, 4,4′-diaminodiphenylmethane, carbonic acid, and thionyl dichloride were purchased from Sinopharm Chemical Reagent Co. 4,4′-(1,4-phenylenediisopropylidene)bisaniline, 4-bromobenzene carboxylic acid and OV-POSS were purchased from Aldrich. 1,4-dioxane, tetrahydrofuran (THF) and toluene were distilled from sodium benzophenoneketyl immediately prior to use.

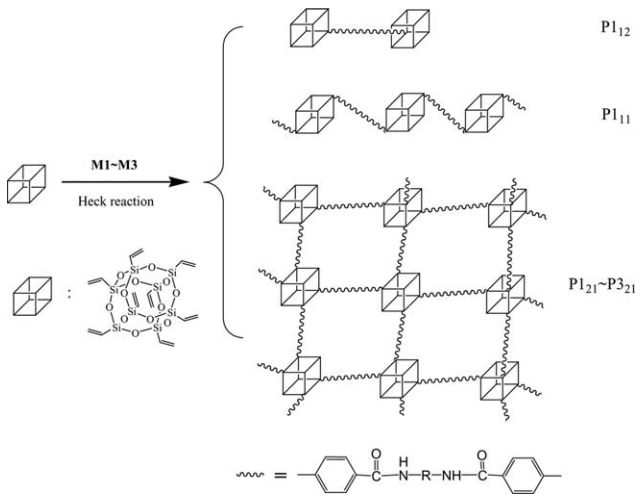

Scheme 2. Synthetic route of the POSS-based hybrids.

Characterization

FTIR spectra were recorded in the region of 4000–400 cm^{-1} on a Nicolet NEXUS 870 FTIR spectrophotometer using KBr disks at room temperature. ^{1}H NMR (400 MHz) and ^{29}Si NMR (79.49 MHz) spectra were measured on a BrukerAV-400 NMR spectrometer. Tetramethylsilane (TMS) was chosen as the internal reference for the ^{1}H NMR analysis in chloroform-*d* solvent. The cross-polarization method was used to obtain the solid-state ^{29}Si NMR spectra. Thermal analysis of the monomers and hybrids were performed on a Perkin Elmer Thermogravimetric analysis (TGA) under nitrogen at a heating rate of 10°C/min. The hybrid thin films were prepared by using spin-coating method from the hybrid solutions (ca. 15 mg/mL) on silicon wafers. Atomic force microscope (AFM, tapping mode) and optical microscope (OM) photographs of the hybrid films were taken in a VeecoNanoscope IV multimode AFM and a CMM-88E metallographic microscope, respectively. The contact-angle measurements of the hybrid films were conducted using OCA40 video optical contact angle meter. Deionized water and glycerol (99%, Shanghai Reagent Co.) were used as the testing liquids. Capacitance measurements were carried out using an Agilent E4980A LCR meter at a frequency of 1 MHz. An array of gold dots approximately 150 nm thick and 2 mm in diameter was deposited onto the film surface by sputtering through a stainless steel mask for capacitance measurements. Film refractive index (n) and thickness (d) were fitted with Cauchy model based on the test results of an ELLIP-SR ellipsometer. The dielectric constant (k) of the film was calculated according to eq. (1).

$$k = C \cdot d/(A \cdot \varepsilon_o) \quad (1)$$

where C is the capacitance of the film; d is the film thickness; A is the area of top gold electrode; and ε_o is the permittivity of free space.

Preparation of Monomers

N,N′-(4,4′-(2,2′-(1,4-Phenylene)bis(propane-2,2-diyl))bis(4,1-phenylene))bis(4-bromobenzamide) (M1). A 150 mL single-necked flask was charged with 4.020 g (20 mmol) 4-

Table I. Parameters of POSS-Based Hybrids

Samples	$n_{M/POSS}$ Feed ratio	m^a ^{1}H NMR	m^a ^{29}Si NMR	T_d[b](°C)	dielectric constant (ε_r) (1 MHz)	refractive index (n)[c] (650 nm)
P1$_{12}$	1 : 2	1.12	1.06	428.6	2.21	1.431
P1$_{11}$	1 : 1	2.22	2.18	416.1	2.39	1.503
P1$_{21}$	2 : 1	3.94	3.92	409.4	2.47	1.523
P2$_{21}$	2 : 1	3.90	3.84	400.6	2.63	1.556
P3$_{21}$	2 : 1	3.84	3.82	371.3	2.87	1.622

[a] The average number of reacted Si–CH=CH bonds of one OV-POSS molecule.
[b] Thermal analyses of the polymers were performed on TGA under nitrogen at a heating rate of 10°C/min.
[c] Refractive index of the hybrid nanocomposites films were fitted with Cauchy model according to test results of ellipsometer.

bromobenzene carboxylic acid and 50 mL anhydrous 1,4-dioxane with a drying tube connected to the condensing unit, which was stirred to form a transparent solution. Then excessive amount of $SOCl_2$ and a few drops of DMF were added, and the solution was refluxed at 60°C for 5 h. The solution color gradually turned into reddish brown during the reaction process. After the reaction finished, the reflux device was transformed into a vacuum distillation unit to remove 1,4-dioxane and $SOCl_2$, and straw yellow solids were obtained. About 40 mL anhydrous THF and 3 mL Et_3N were added into the flask to dissolve straw yellow solids, then 2.756 g (8 mmol) 4,4′-(1,4-phenylenediisopropylidene)bisaniline was slowly added into the above solution, which was refluxed at 75°C for 12 h. After the reaction, the solvent was removed by vacuum distillation method, and the reaction mixtures were processed with ultrasonic cleaning in deionized water. Then the dry crude product was subjected to Al_2O_3 column chromatography. Elution of the column with a mixture of ethyl acetate and petroleum ether (1 : 5, v/v) gave 4.775 g gray-white crystals in 84% yield. FTIR (KBr, cm^{-1}): 3305 (N–H), 3032 (Ar–H), 2969, 2928, 2873 (CH_3), 1648 (C=O), 1598, 1536, 1514 (CH=CH of Ar ring), 837 (p-Ar). ^{1}H NMR (400 MHz, DMSO-d_6), δ (TMS, ppm): 10.24 (s, 2H, CON*H*), 7.89 (d, 4H, J = 7.2Hz, H^2), 7.74 (d, 4H, J =12.4 Hz, H^1), 7.64 (d, 4H, J = 8.0 Hz, H^3), 7.20 (d, 4H, J = 7.6Hz, H^4), 7.09 (br, 4H, H^5), 1.60 (br, 12H, C*H*$_3$).

N,N′-(4,4′-Methylenebis(4,1-phenylene))bis(4-bromobenzamide) (M2). This was prepared as above from 4,4′-diaminodiphenylmethane and 4-bromobenzene carboxylic acid. Monomer M2 was obtained as yellow crystals in 83% yield. FTIR (KBr, cm^{-1}): 3294 (N–H), 3041 (Ar–H), 2908, 2835 (CH_2), 1658 (C=O), 1591, 1525 (CH=CH of Ar ring), 842 (p-Ar). ^{1}H NMR (400 MHz, DMSO-d_6), δ (TMS, ppm): 10.27 (s, 2H, CON*H*), 7.90 (d, 4H, J = 9.6Hz, H^2), 7.74 (d, 4H, J =8.4 Hz, H^1), 7.67 (d, 4H, J = 8.8 Hz, H^3), 7.21 (d, 4H, J = 9.2Hz, H^4), 3.90 (d, 2H, J = 4.8Hz, C*H*$_2$).

N,N′-(1,4-Phenylene)bis(4-bromobenzamide) (M3). This was prepared as above from 1,4-benzenediamine and 4-bromobenzene carboxylic acid. Monomer M3 was obtained as yellow crystals in 79% yield. FTIR (KBr, cm^{-1}): 3326 (N–H), 3045 (Ar–H), 1647 (C=O), 1590, 1541, 1521 (CH=CH of Ar ring), 837 (p-Ar). ^{1}H NMR (400 MHz, DMSO-d_6), δ (TMS, ppm): 10.32 (s, 2H, CON*H*), 7.87 (d, 4H, J = 8.4Hz, H^2), 7.74 (q, 4H, J =14.4 Hz, H^{1,3}), 3.90 (d, 2H, J = 4.8Hz, C*H*$_2$).

Design and Preparation of POSS-Based Hybrids. The hybrids are prepared via a conventional Heck reaction by using $Pb(Ac)_2$ as a catalyst and K_2CO_3 as acid binding agent (Scheme 2).[41] The reactions were carried out under nitrogen atmosphere in the Schlenk polymerization tube. The hybrids with different molecular architectures including dumbbell-type (P1$_{12}$, defined as the polymer obtained based on reaction of M1 (P1) with OV-POSS at a feed ratio of 1 : 2. The other abbreviations of hybrids are similar with P1$_{12}$), bead-type (P1$_{11}$), and cross-linked (P1$_{21}$) structures were prepared only by varying the feeding ratio of M1 and OV-POSS (Table I). The typical example of experimental procedure for bead-type hybrids of P1$_{11}$ was given as follows: A mixture of 0.711 g M1 (1.0 mmol), 0.633g of OV-POSS (1.0 mmol), 0.011 g of $Pb(OAc)_2$ (0.05 mmol), 0.023 g of $P(Ph)_3$ (0.10 mmol), and 0.414 g of K_2CO_3 (3.0 mmol) was placed in a 100 mL Schlenk tube with a side arm. The Schlenk tube was evacuated under vacuum and then flushed with dry nitrogen for three times. After 20 mL fresh distilled dimethylformamide was injected, the reaction mixture was refluxed at 130°C under nitrogen for 10 h and cooled to room temperature. The mixture was then diluted with 100 mL water and filtered. The precipitate was washed with sufficient toluene.

P1$_{11}$: Brown powder, yield: 53%. FTIR (KBr, cm^{-1}): 3317 (N–H), 3066 (Ar–H), 2963, 2930, 2855 (CH_3), 1652 (C=O), 1599, 1521 (CH=CH of Ar ring), 1112 (Si–O–Si), 776 (C–Si). ^{1}H NMR (400 MHz, DMSO-d_6), δ (TMS, ppm): 10.27 (br, H, CON*H*), 7.90 (br, H, H^2), 7.53 (br, H, H^{1,3}), 7.17 (br, H, H^{4,5}), 5.95 (br, H, Si–C*H*=C*H*$_2$ and Si–C*H*=C*H*$_2$–Ar), 1.62 (br, H, C*H*$_3$). ^{29}Si NMR (79.49 MHz, solid), δ: −72.2 (s, Si–CH=CH–Ar), −80.1 (s, Si–CH=CH$_2$).

P1$_{12}$: Brown powder, yield: 55%. FTIR (KBr, cm^{-1}): 3315 (N–H), 3064 (Ar–H), 2960, 2929, 2857 (CH_3), 1653 (C=O), 1598, 1517 (CH=CH of Ar ring), 1113 (Si–O–Si), 775 (C–Si). ^{1}H NMR (400 MHz, DMSO-d_6), δ (TMS, ppm): 10.28 (br, H, CON*H*), 7.91 (br, H, H^2), 7.52 (br, H, H^{1,3}), 7.15 (br, H, H^{4,5}), 5.94 (br, H, Si–C*H*=C*H*$_2$ and Si–C*H*=C*H*$_2$–Ar), 1.61 (br, H, C*H*$_3$). ^{29}Si NMR (79.49 MHz, solid), δ: −72.6 (s, Si–CH=CHR), −79.7 (s, Si–CH=CH$_2$).

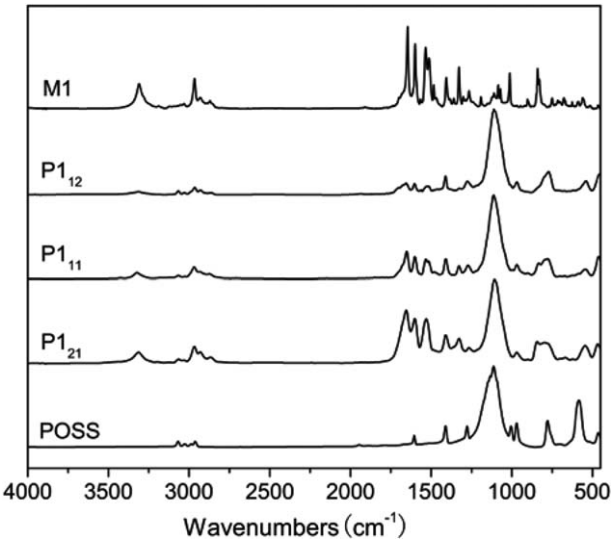

Figure 1. IR spectra of M1, $P1_{12}$, $P1_{11}$, $P1_{21}$, and POSS.

$P1_{21}$: Brown powder, yield: 48%. FTIR (KBr, cm^{-1}): 3316 (N–H), 3064 (Ar–H), 2967, 2935, 2858 (CH_3), 1656 (C=O), 1601, 1530 (CH=CH of Ar ring), 1110 (Si–O–Si), 781 (C–Si). ^{1}H NMR (400 MHz, DMSO-d_6), δ (TMS, ppm): 10.29 (br, H, CON*H*), 7.92 (br, H, H^2), 7.52 (br, H, $H^{1,3}$), 7.16 (br, H, $H^{4,5}$), 5.97 (br, H, Si–C*H*=CH_2 and Si–C*H*=CH_2–Ar), 1.62 (br, H, CH_3). ^{29}Si NMR (79.49 MHz, solid), δ: −71.9 (s, Si–CH=CHR), −80.0 (s, Si–CH=CH_2).

$P2_{21}$: Brown powder, yield: 48%. FTIR (KBr, cm^{-1}): 3315 (N–H), 3052 (Ar–H), 2925, 2854 (CH_2), 1658 (C=O), 1598, 1526 (CH=CH of Ar ring), 1110 (Si–O–Si), 786 (C–Si). ^{1}H NMR (400 MHz, DMSO-d_6), δ (TMS, ppm): 10.28 (br, H, CON*H*), 7.88 (br, 4H, H^2), 7.53 (br, H, $H^{1,3}$), 7.19 (br, H, H^4), 5.99 (br, H, Si–C*H*=CH_2 and Si–C*H*=CH_2–Ar), 3.92 (br, H, CH_2). ^{29}Si NMR (79.49 MHz, solid), δ: −71.7 (s, Si–CH=CHR), −80.1 (s, Si–CH=CH_2).

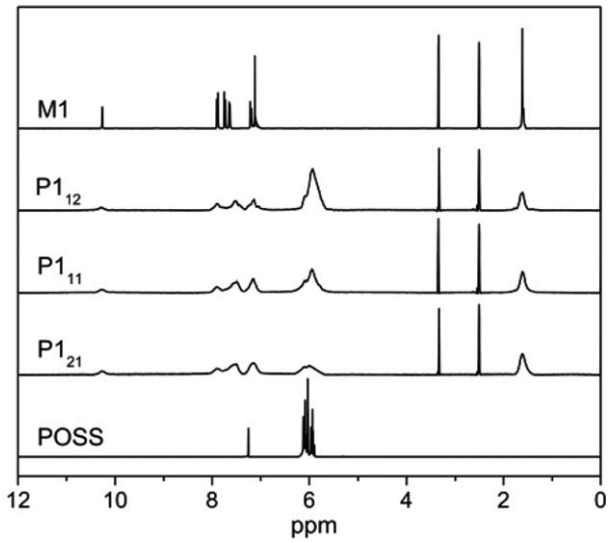

Figure 2. ^{1}H NMR spectra of M1, $P1_{12}$, $P1_{11}$, $P1_{21}$, and POSS.

$P3_{21}$: Brown powder, yield: 48%. FTIR (KBr, cm^{-1}): 3324 (N–H), 3070 (Ar–H), 2948, 2860 (C–H), 1652 (C=O), 1604, 1540 (CH=CH of Ar ring), 1112 (Si–O–Si), 782 (C–Si). ^{1}H NMR (400 MHz, DMSO-d_6), δ (TMS, ppm): 10.28 (br, H, CON*H*), 7.87 (br, H, H^2), 7.57 (br, H, $H^{1,3}$), 6.07 (br, H, Si–C*H*=CH_2 and Si–C*H*=CH_2–Ar). ^{29}Si NMR (79.49 MHz, solid), δ: −70.9 (s, Si–CH=CHR), −79.9 (s, Si–CH=CH_2).

RESULTS AND DISCUSSION

The hybrids with different architectures were prepared via Heck reaction by varying the feed ratio. It is found that $P1_{12}$ (feed ratio = 1 : 2) and $P1_{11}$ (feed ratio = 1 : 1) hybrids have good solubility in common solvent such as 1,4-dioxane, DMF, and DMSO, while $P1_{21}$ (feed ratio = 2 : 1) is only partly soluble in the above solvents, indicating that the cross-linked structure was formed. When the feed ratio is at 3 : 1 or 4 : 1, the resultant hybrids are almost completely insoluble in all common organic solvents, which may be due to the formation of highly cross-linked structures.

Structure Characterization of POSS-Based Hybrids

Spectral characterization was utilized to investigate the structures of target materials. Figure 1 displays the IR spectra of the nanocomposite $P1_{12}$, $P1_{11}$, and $P1_{21}$ ($P1_{xy}$). For the convenience of comparison, the IR spectra of POSS and monomer M1 were also presented. It can be seen from Figure 1 that monomer M1 displays strong N–H stretching vibration absorption of secondary amine and C=O stretching vibration absorption at 1648 cm^{-1}. POSS presents Si–O–Si stretching vibrational peak at 1108 cm^{-1}. The FTIR spectra of hybrid materials of $P1_{xy}$ show the characteristic stretching vibration absorption band of Si–O–Si at ~1112 cm^{-1}, N–H stretching vibration absorption of secondary amine at 3316cm^{-1} and a very strong C=O stretching vibration absorption at 1653 cm^{-1}, demonstrating the Heck coupling reaction between M1 and POSS was effectively actualized. In addition, with increasing the feed ratio of monomer M1 to POSS, the intensity ratio of N–H and C=O stretching vibration absorption to Si–O–Si absorption peak increases from $P1_{12}$, $P1_{11}$ to $P1_{21}$, which illustrates that the POSS content of $P1_{xy}$ can be tuned by altering the feed ratio.

Figure 2 shows ^{1}H NMR spectra of M1, POSS, and $P1_{xy}$ hybrids. Obviously, the spectra of all resulting $P1_{xy}$ hybrids display the broad vibration bands at δ10.28, 6.98~8.02, and 1.61 ppm corresponding to the characteristic proton absorptions of CON*H*, $H^{1\sim6}$ of Ar, and CH_3 in the M1, and another strong broad vibration bands at δ5.61~6.22 ppm corresponding to the characteristic proton absorptions of CH_2=C*H*–Si and Ar–C*H*=C*H*–Si. In addition, the broad vibration band at δ5.61~6.22 displays a gradual decrease from $P1_{12}$, $P1_{11}$ to $P1_{21}$, demonstrating that the POSS content decreases, which is consistent with the results of FTIR. Supposing that the average number of the reacted Ar–C*H*=C*H*–Si of each OV-POSS molecule in the hybrids is *m*, so the number of the total proton (CH_2=C*H*–Si and Ar–C*H*=C*H*–Si) of each POSS molecule in the hybrids is 24-*m*, whose integration area is defined as A_{poss}. Two broad peaks appear in the range of 7.35~8.02 ppm, which

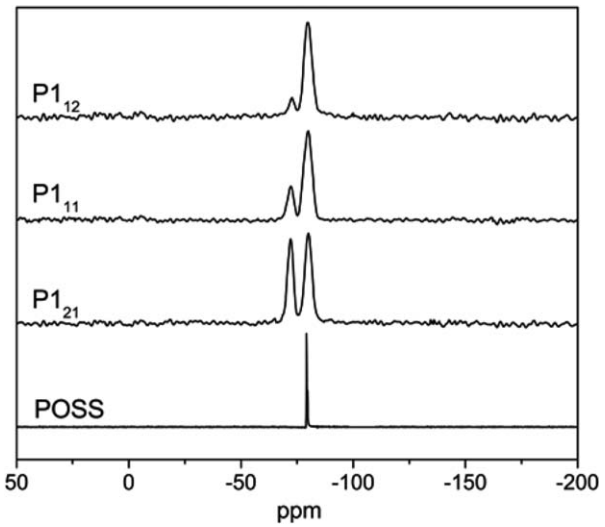

Figure 3. ^{29}Si NMR spectra of $P1_{12}$, $P1_{11}$, $P1_{21}$, and POSS.

correspond to resonant absorption bands of H[1,2,3] of Ar in monomers (see Scheme 1), with the number of protons in each monomer being 12, and the integration area is defined as A_M. Therefore, based on integrated area of ^{1}H NMR spectra, the average number of the reacted CH_2=CH–Si(Ar–CH=CH–Si) of each OV-POSS molecule in the hybrids can be calculated according to eq. (2):

$$m = \frac{24A_M}{6A_{POSS} + A_M} \quad (2)$$

The results are listed in Table I. It can be seen that the average number of reacted CH_2=CH–Si of OV-POSS for P_{21} is about ca. 1 when the feed ratio of monomer to OV-POSS is 1 : 2, demonstrating that the resultant hybrids mainly consist of dumbbell-type structural molecules. The average number of reacted Ar–CH=CH–Si of OV-POSS is ca. 2 when the feed ratio is 1 : 1, suggesting that the resulting hybrids mainly consist of bead-type structural molecules considering the steric hindrance. At a feed ratio of 2 : 1, the average number of reacted CH_2=CH–Si is about ca. 4, confirming that the cross-linked structural hybrid composites are yielded. It demonstrated that the molecular architecture of the hybrids can be tuned by simply varying the feeding ratio of the reactants.

The cross-polarization method was used to obtain ^{29}Si MAS NMR spectra, as shown in Figure 3. The ^{29}Si NMR spectra of these hybrids show two resonance absorption peaks at ~–72 and −80 ppm, which are attributed to Si resonance absorption of *Si*–CH=CH–Ar and unreacted *Si*–CH=CH_2, respectively. The relative intensity of resonance absorption of Si–CH=CH_2–Ar gradually increases from $P1_{12}$, $P1_{11}$ to $P1_{21}$. This is consistent with the results of IR and ^{1}H NMR spectra. On the basis of the integrations for solid-state ^{29}Si NMR spectra, the average number of substituent group of POSS can also be calculated using the following eq. (3) and the results were summarized in Table I.

$$m = \frac{A_{Si\text{-}CH=CH\text{-}Ar}}{A_{Si\text{-}CH=CH} + A_{Si\text{-}CH=CH\text{-}Ar}} \times 8 \quad (3)$$

Here *A* represents the absorbance peak area in the ^{29}Si NMR spectra of the hybrids. The values of *m* obtained by ^{29}Si NMR spectra are consistent with that from ^{1}H NMR spectra (Table I), further supporting that the molecular architecture of hybrid composites can be effectively adjusted by varying the feed ratio of monomer to OV-POSS.

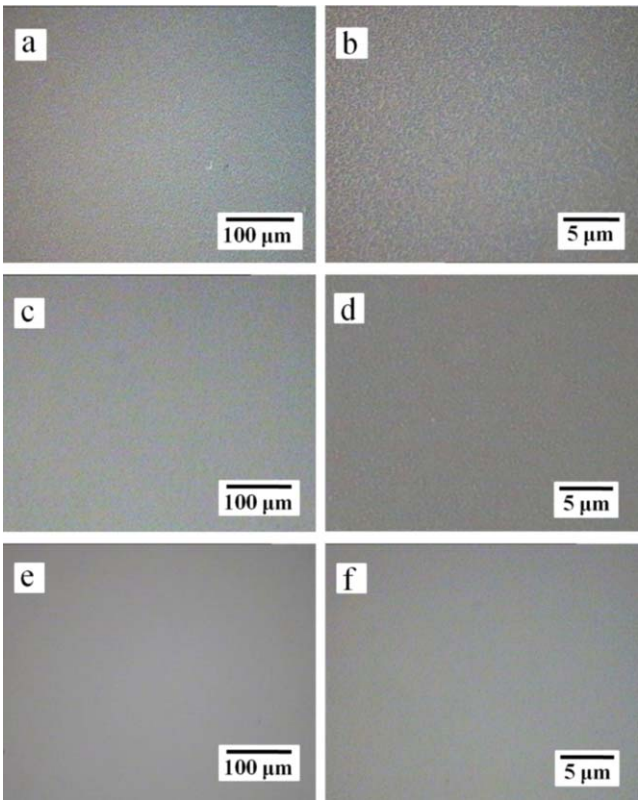

Figure 4. OM micrographs at different magnifications (a) 200×, (b) 3200× for $P1_{12}$, (c) 200×, (d) 3200× for $P1_{11}$, and (e) 200×, (f) 3200× for $P1_{21}$ thin films. [Color figure can be viewed in the online issue, which is available at wileyonlinelibrary.com.]

Film Formability of POSS-Based Hybrids

Since the as-synthesized $P1_{12}$, $P1_{11}$, and $P1_{21}$ can be only dissolved in polar solvents such as 1,4-dioxane, DMF, and DMSO with high boiling points. Even the 1,4-dioxane, its boiling point is as high as 101°C, which makes it difficult to volatilize. The uniform and completed film cannot be obtained on the substrates by spin-coating at room temperature. Therefore, we put the substrate (steel or silicon wafer) into the oven, heating up to a certain temperature lower than the boiling point of the solvent by 20~40°C. After that, the substrate was taken out swiftly and spin-coated to form film. The microstructures of the hybrid films were characterized using OM and AFM.

The OM images with a 200× magnifications were displayed in the Figure 4(a,c,e), which correspond to hybrid materials of $P1_{12}$, $P1_{11}$, and $P1_{21}$. In such a magnification, we found that the film was integral and the surface uniformity was improved gradually from $P1_{12}$, $P1_{11}$ to $P1_{21}$. Further investigation at a magnification of 3200× shows that the film has obvious fine

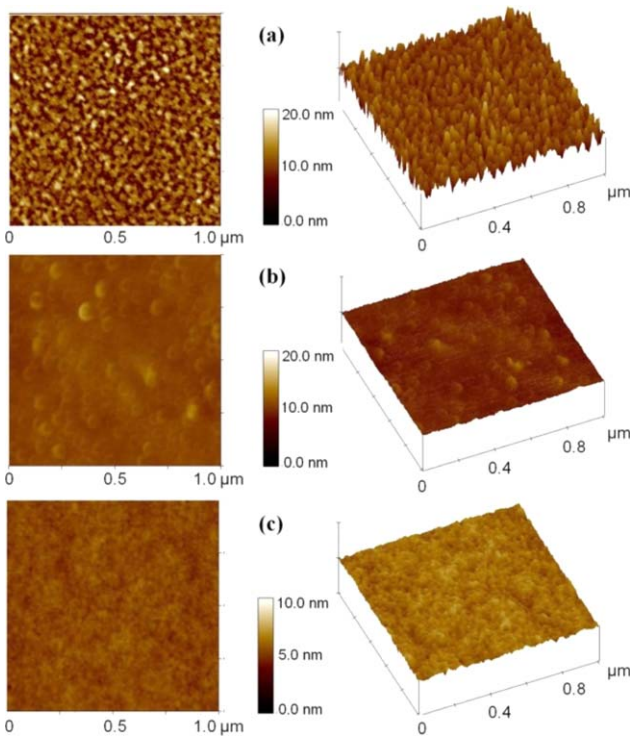

Figure 5. Atomic force microscope images of (a) $P1_{12}$, (b) $P1_{11}$, and (c) $P1_{21}$ thin films. [Color figure can be viewed in the online issue, which is available at wileyonlinelibrary.com.]

lines in $P1_{12}$ film [Figure 4(b)] and small dots in $P1_{11}$ film [Figure 4(d)] while Pl_{21} film [Figure 4(f)] still remains smooth. It demonstrates that the film formability of POSS-based hybrids are improved from dumbbell-type, bead-type to low cross-linked.

In order to observe the film formability of the hybrid materials at nanoscale, AFM was used to scan the surface of the hybrid films. Figure 5 shows the AFM images of the $P1_{12}$, $P1_{11}$, and $P1_{21}$ films, it can be seen that the microstructures exhibit large difference among the three different structural hybrids. $P1_{12}$ film is composed of nanoscale particles with great roughness and $P1_{11}$ film shows "island hill" structure. However, $P1_{21}$ film is very smooth and there are no particle aggregates or "island hill" structures. The results confirm that $P1_{21}$ shows better film formability than the others, which is consistent with the OM results. The dumbbell-type $P1_{12}$ and bead-type $P1_{11}$ hybrid materials are inclined to form particles at tens of nanometers owing to the strong POSS–POSS interaction. However, low cross-linked $P1_{21}$ hybrid materials was formed through chemical bonding with three-dimensional coupling, hence effectively blocking the interactions between POSS molecules, and generating POSS-based well-dispersed organic-inorganic hybrid materials.

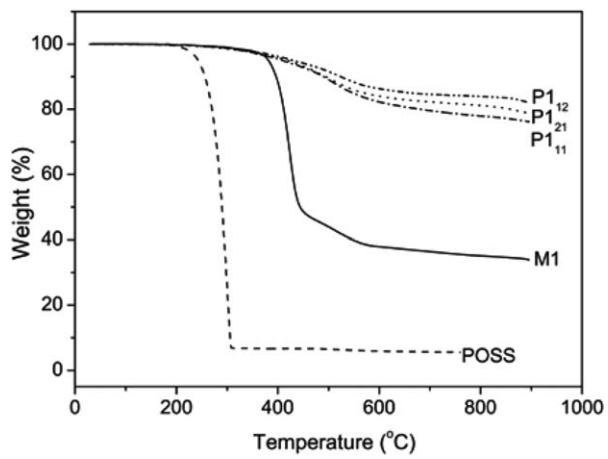

Figure 6. TGA of M1, POSS, $P1_{12}$, $P1_{11}$, and $P1_{21}$ hybrids.

Thermal Stability

The thermal stability of the resulting hybrids was evaluated by TGA under nitrogen atmosphere at a heating rate of $10°C \cdot min^{-1}$. Figure 6 shows the TGA thermogram of $P1_{xy}$ hybrids. For comparison, the TGA curves of OV-POSS and M1 monomer are also given, and the data are summarized in Table I. OV-POSS begins to lose weight at 242.7°C, probably due to its sublimation.[38] For M1 monomer, the initial thermal decomposition occurs at about 381.6°C. However, $P1_{xy}$ hybrids display a largely reinforced decomposition temperature (T_d) over 409.4°C, much higher than the T_d of either OV-POSS or M1 monomer. This clearly indicates that the chemical bonding between OV-POSS and M1 molecules can prevent the sublimation of OV-POSS and the hollow Si–O–Si cage can efficiently slow down the thermal conductivity to protect linking organic chains in the materials, improving the thermal property of the resultant hybrids. However, it is found that T_d of the hybrids is not simply increased with the POSS content, which is also closely related with the molecular architecture. For example, dumbbell-type $P1_{12}$ hybrids have the highest POSS content as well as the highest T_d. However, the T_d of bead-type $P1_{11}$ hybrids is lower than that of cross-linked $P1_{21}$ hybrids, although the POSS content of $P1_{11}$ hybrids is higher than that of $P1_{21}$ hybrids. This may be related to intense aggregation of POSS in the $P1_{11}$ hybrids, which is confirmed by the OM and AFM results. Additionally, the T_d of $P2_{21}$ and $P3_{21}$ hybrids are 400.6°C and 371.3°C, much higher than the T_d of M2 (356.5°C) and M3 (330.1°C), respectively, demonstrating that the incorporation of POSS significantly improves the thermal stability. Compared the Td of $P1_{21}$, $P2_{21}$, and $P3_{21}$ with the same molecular architecture, it indicates that the chemical structure of linking organic chains plays an important role in the thermal decomposition temperature of the hybrids.

The Mechanism of the Dielectric Constant Variation

Effect of Molecular Architecture. The refractive index (n) and thickness (d) of the hybrid thin films were measured by an ELLIP-SR ellipsometer and their low dielectric constants (k) were determined by capacitance method at a frequency of 1 MHz. For comparison, the dielectric constant (k) and refractive index (n) of $P1_{xy}$, $P2_{21}$, and $P3_{21}$ hybrids are listed in Table I. It is clearly seen that k values of dumbbell-type $P1_{12}$, bead-type $P1_{11}$, and cross-linked $P1_{21}$ increase from 2.21, 2.39 to 2.47. Considering their POSS content (molar percentage) being 65.4%, 47.8%, and 33.8%, respectively, based on the result of ^{29}Si NMR spectra, POSS content is the main contribution to the variation of dielectric constant. Because POSS has lower intrinsic dielectric constant compared with the polar linking

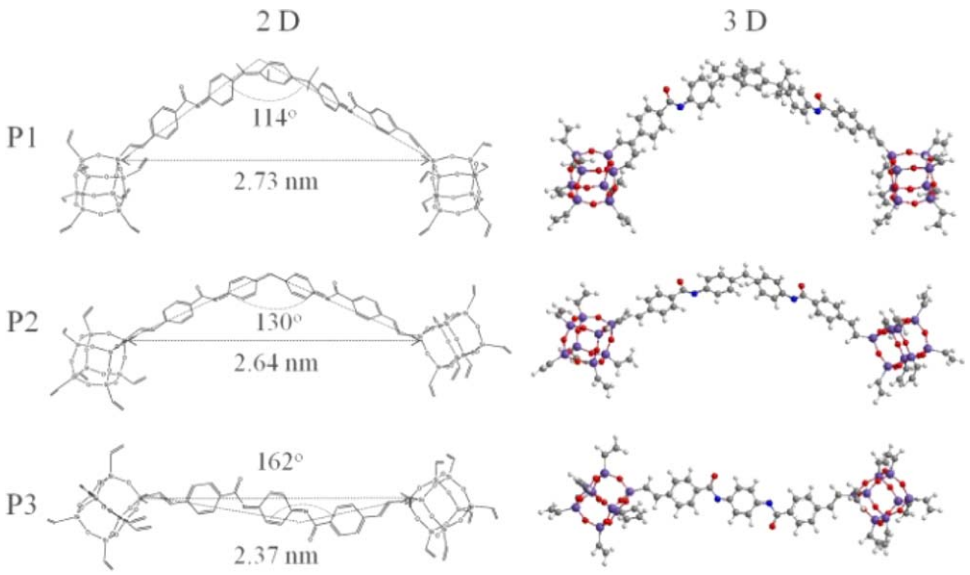

Figure 7. The geometrical characteristics of linking chains in $P1_{21}$, $P2_{21}$, and $P3_{21}$ hybrids. [Color figure can be viewed in the online issue, which is available at wileyonlinelibrary.com.]

organic chains and the incorporation of POSS into the hybrids brings high porosity due to its bulky steric hindrance, the higher POSS content results in a lower dielectric constant. To further explore the influence of molecular architecture on the *k* values, we compared the difference in POSS content and dielectric constant of the hybrids among the three architectures. The molar percentage of POSS in $P1_{11}$ is lower than that in $P1_{12}$ by 17.6%, resulting in a decrease of *k* by 0.18. However, the molar percentage of POSS in $P1_{21}$ is lower than that in $P1_{11}$ by 14.0%, which just leading to a decrease of *k* by only 0.08. This suggests that the porosity induced by every OV-POSS unit in the cross-linked Pl_{21} is higher than that in bead-type $P1_{11}$ hybrid materials. That is, the molecular architectures have an important effect on the porosity or free volume in the resultant hybrids.[42] Compared with one dimensional dumbbell-type and bead-type hybrid materials, the three-dimensional cross-linked hybrids can reduce the interactions between POSS and linking organic chains, leading to higher porosity for each POSS unit in the resultant hybrids.

Effect of Chemical Structure. Table I shows *k* values of cross-linked $P1_{21}$, $P2_{21}$, and $P3_{21}$ being 2.47, 2.63, and 2.87, respectively. These hybrids possess the same molecular architecture and similar POSS molar contents, so the difference of their dielectric constants can be attributed to the different chemical structures of the linking organic chains. With the increasing proportion of the polar O=CNH group in the linking organic chains of $P1_{21}$, $P2_{21}$, and $P3_{21}$ hybrids, the polarity of the corresponding hybrids increases, which is confirmed in the following analysis of the surface energy. In order to further investigate the influence of the linking organic chains on the dielectric constant, we adopted two calculation steps to calculate the geometrical characteristics of the linking organic chains in cross-linked $P1_{21}$, $P2_{21}$, and $P3_{21}$ hybrids. First, all complexes were optimized using the AM1 semi-empirical method implemented in the Gaussian 03 suite of program. Based on the resultant geometries, the full geometry reoptimizations were performed at the HF/6–31G level of theory.

Figure 7 displays the calculated two (2D) and three (3D) dimensional geometrical characteristics of linking chains between OV-POSSs in $P1_{21}$, $P2_{21}$, and $P3_{21}$ hybrids. It is clearly observed that the distance between OV-POSSs in $P1_{21}$, $P2_{21}$, and $P3_{21}$ hybrids slightly decreases from 2.73, 2.64 to 2.37 nm due to the different size of their linking chains. Moreover, the bending angles of the linking chains between OV-POSSs change from 114°, 130° to 162° in $P1_{21}$, $P2_{21}$, and $P3_{21}$ hybrids, respectively. The longer distance between OV-POSSs and smaller bending angle are difficult for densely packing, thus beneficial to produce higher porosity in the hybrid materials, resulting in a lower dielectric constant. Therefore, such dielectric constant variation in $P1_{21}$, $P2_{21}$, and $P3_{21}$ hybrids can be attributed to the cooperative effect of an increasing content of polar groups and a decreasing porosity of the hybrid materials. In addition, the variation trend of refractive indices is consistent with dielectric constants in all the hybrid materials.

It is well understood that the surface free energy of films is closely to the polarizability and intra/interactions between molecules. To further investigate the mechanism for the variation of the dielectric constant, the surface free energy (γ_s), including polar component (γ_s^P), and dispersive component (γ_s^d), of these resulting hybrids were determined according to Wu's harmonic mean method and the data of contact-angle (water and glycerol) measurements of these hybrid films.[43] As seen in the Table II, the contact angles gradually decrease from dumbbell-type $P1_{12}$, bead-type $P1_{11}$ to cross-linked $P1_{21}$, $P2_{21}$, and $P3_{21}$, indicating an increase of hydrophilicity. Synchronously, the corresponding surface free energy (γ_s) increases, so do polar component (γ_s^P) and dispersive component (γ_s^d). Compared with γ_s^d, γ_s^P predominates the increase of γ_s, which reveals that

Table II. Surface Properties of POSS-Based Hybrids

Samples	Θ (°±σ)				
	Water	Glycerol	γ_s (mN/m)[a]	γ_s^d (mN/m)[a]	γ_s^p (mN/m)[a]
$P1_{12}$	98.8 ± 1.1	93.5 ± 0.9	20.0	9.39	10.6
$P1_{11}$	93.5 ± 0.8	88.4 ± 1.1	22.8	10.3	12.5
$P1_{21}$	88.2 ± 1.4	84.3 ± 0.7	25.6	10.5	15.1
$P2_{21}$	82.8 ± 1.2	80.2 ± 0.8	28.7	10.8	17.9
$P3_{21}$	77.5 ± 1.1	75.0 ± 1.1	32.0	12.1	19.9

[a] Calculated with Wu's harmonic mean method.

the polarizability of the hybrids successively increases from dumbbell-type $P1_{12}$, bead-type $P1_{11}$ to cross-linked $P1_{21}$, $P2_{21}$, and $P3_{21}$. Apparently, the variation trend of the surface free energy in the resultant hybrids is in agreement with that of their dielectric constants. Similar results were obtained in Ye's work.[29]

Finally, we would like to compare our results with that in the previous works. Leu *et al.*[20] first introduced POSS into polyimide matrix, the dielectric constant can be decreased to 2.32 from 3.26 when the molar percentage of POSS was 35%. Similarly, Chen *et al.*[25] grafted POSS onto polyimide, the dielectric constant of 2.2 was obtained. POSS was further incorporated into the main chains of polyimide in Wu's work.[26] The dielectric constant can be reduced to 2.36. Lee *et al.*[17] prepared POSS-based hybrids with network structure, the lowest dielectric constant was 2.65. In this work, the dielectric constants were in the range of 2.21–2.87, comparable with the above values. Most importantly, this work doesn't focus on the low dielectric constant properties, but the effect of chemical structure and molecular architecture of POSS-based hybrids on the dielectric constant, which is very significant in molecular design of low dielectric constant hybrids.

CONCLUSIONS

In this work, POSS-based inorganic-organic hybrid materials with different architectures, including dumbbell-type, bead-type, and cross-linked network, and linking organic chains were prepared via Heck reaction by simply varying the feed ratio. All the hybrids exhibit good thermal stability and low dielectric constant. Specially, the low cross-linked hybrid materials show excellent film formability. The dielectric constant variation of the hybrids is dominated by POSS content, while molecular architecture and chemical structure of organic chains also play an important role. It is expected that the understanding here about the dependence of the low dielectric constant on the molecular structure and architecture will help the design of new POSS-based hybrid materials with desirable low dielectric constants.

ACKNOWLEDGMENTS

This research was financially supported by the National Natural Science Fund of China (Grant Nos. 51073031, 20971021, and 20974018), Shanghai Municipal Natural Science Foundation for Youths (No.12ZR144100), and "Chen Guang" project (No.12CG37) supported by Shanghai Municipal Education Commission and Shanghai Education Development Foundation.

REFERENCES

1. Cordes, D. B.; Lickiss, P. D.; Rataboul, F. *Chem. Rev.* **2010**, *110*, 2081.
2. Xu, H. Y.; Kuo, S. W.; Lee, J. S.; Chang, F. C. *Macromolecules* **2002**, *35*, 8788.
3. Xu, H. Y.; Yang, B. H.; Wang, J. F.; Guang, S. Y.; Li, C. *Macromolecules* **2005**, *38*, 10455.
4. Baldi, F.; Bignotti, F.; Fina, A.; Tabuani, D.; Ricco, T. *J. Appl. Polym. Sci.* **2007**, *105*, 935.
5. He, Q.; Song, L.; Hu, Y.; Zhou, S. *J. Mater. Sci.* **2009**, *44*, 1308.
6. Zhang, W. C.; Li, X. M.; Yang, R. J. *J. Appl. Polym. Sci.* **2012**, *124*, 1848.
7. Augustine, B. H.; Hughes, W. C.; Zimmermann, K. J.; Figueiredo, A. J.; Guo, X. W.; Chusuei, C. C.; Maidment, J. S. *Langmuir* **2007**, *23*, 4346.
8. Lee, Y. J.; Huang, J. M.; Kuo, S. W.; Chang, F. C. *Polymer* **2005**, *46*, 10056.
9. Zeng, L.; Liang, G. Z.; Gu, A. J.; Yuan, L.; Zhuo, D. X.; Hu, J. T. *J. Mater. Sci.* **2012**, *47*, 2548.
10. Ke, F. Y.; Zhang, C.; Guang, S. Y.; Xu, H. Y. *J. Appl. Polym. Sci.* **2013**, *127*, 2628.
11. Imae, I.; Kawakami, Y. *J. Mater. Chem.* **2005**, *15*, 4581.
12. Lo, M. Y.; Zhen, C. G.; Lauters, M.; Jabbour, G. E.; Sellinger, A. *J. Am. Chem. Soc.* **2007**, *129*, 5808.
13. Yan, Y. X.; Wang, J.; Liu, T. B.; Wang, X.; Su, X. Y.; Feng, Y. *J. Appl. Polym. Sci.* **2014**, *131*, 40246.
14. Su, X. Y.; Guang, S. Y.; Xu, H. Y.; Yang, J. Y.; Song, Y. L. *Dyes Pigments* **2010**, *87*, 69.
15. Su, X. Y.; Guang, S. Y.; Li, C. W.; Xu, H. Y.; Liu, X. Y.; Wang, X.; Song, Y. L. *Macromolecules* **2010**, *43*, 2840.
16. Su, X. Y.; Xu, H. Y.; Deng, Y.; Li, J. R.; Zhang, W.; Wang, P. *Mater. Lett.* **2008**, *62*, 3818.
17. Lee, Y. J.; Huang, J. M.; Kuo, S. W.; Lu, J. S.; Chang, F. C. *Polymer* **2005**, *46*, 173.
18. Geng, Z.; Huo, M. X.; Mu, J. X.; Zhang, S. L.; Lu, Y. N.; Luan, J. S.; Huo, P. F.; Du, Y. L.; Wang, G. B. *J. Mater. Chem. C* **2014**, *2*, 1094.

19. Hartmann-Thompson, C.; Merrington, A.; Carver, P. I.; Keeley, D. L.; Rousseau, J. L.; Hucul, D.; Bruza, K. J.; Thomas, L. S.; Keinath, S. E.; Nowak, R. M.; Katona, D. M.; Santurri, P. R. *J. Appl. Polym. Sci.* **2008**, *110*, 958.

20. Leu, C. M.; Reddy, G. M.; Wei, K. H.; Shu, C. F. *Chem. Mater.* **2003**, *15*, 2261.

21. Seckin, T.; Koytepe, S.; Adiguzel, H. I. *Mater. Chem. Phys.* **2008**, *112*, 1040.

22. Leu, C. M.; Chang, Y. T.; Wei, K. H. *Macromolecules* **2003**, *36*, 9122.

23. Leu, C. M.; Chang, Y. T.; Wei, K. H. *Chem. Mater.* **2003**, *15*, 3721.

24. Chen, Y. W.; Kang, E. T. *Mater. Lett.* **2004**, *58*, 3716.

25. Chen, Y. W.; Chen, L.; Nie, H. R.; Kang, E. T. *J. Appl. Polym. Sci.* **2006**, *99*, 2226.

26. Wu, S.; Hayakawa, T.; Kikuchi, R.; Grunzinger, S. J.; Kakimoto, M. *Macromolecules* **2007**, *40*, 5698.

27. Wu, S.; Hayakawa, T.; Kakimoto, M.; Oikawa, H. *Macromolecules* **2008**, *41*, 3481.

28. Chen, W. Y.; Ko, S. H.; Hsieh, T. H.; Chang, F. C.; Wang, Y. Z. *Macromol. Rapid. Comm.* **2006**, *27*, 452.

29. Ye, Y. S.; Chen, W. Y.; Wang, Y. Z. *J. Polym. Sci. Pol. Chem* **2006**, *44*, 5391.

30. Wahab, M. A.; Mya, K. Y.; He, C. B. *J. Polym. Sci. Pol. Chem.* **2008**, *46*, 5887.

31. Maier, G. *Prog. Polym. Sci.* **2001**, *26*, 3.

32. Seino, M.; Wang, W. D.; Lofgreen, J. E.; Puzzo, D. P.; Manabe, T.; Ozin, G. A. *J. Am. Chem. Soc.* **2011**, *133*, 18082.

33. Xi, K.; He, H.; Xu, D.; Ge, R. J.; Meng, Z.; Jia, X. D.; Yu, X. H. *Thin Solid Films* **2010**, *518*, 4768.

34. Wu, G. J.; Su, Z. H. *Chem. Mater.* **2006**, *18*, 3726.

35. Decher, G. *Science* **1997**, *277*, 1232.

36. Liu, Y. L.; Fangchiang, M. H. *J. Mater. Chem.* **2009**, *19*, 3643.

37. Wang, C. Y.; Chen, W. T.; Chen, Y. Y.; Zhao, X. Y.; Li, J.; Ren, Q. *Mater. Chem. Phys.* **2014**, *143*, 773.

38. Yang, B. H.; Xu, H. Y.; Yang, Z. Z.; Liu, X. Y. *J. Mater. Chem.* **2009**, *19*, 9038.

39. Yang, B. H.; Xu, H. Y.; Yang, Z. Z.; Zhang, C. *J. Mater. Chem.* **2010**, *20*, 2469.

40. Zhang, C.; Guang, S. Y.; Zhu, X. B.; Xu, H. Y.; Liu, X. Y.; Jiang, M. H. *J. Phys. Chem. C* **2010**, *114*, 22455.

41. Heck, R. F.; Nolley, J. J. P. *J. Org. Chem.* **1972**, *37*, 2320.

42. Wang, Y. Z.; Chen, W. Y.; Yang, C. C.; Lin, C. L.; Chang, F. C. J. *Polym. Sci. Part B: Pol. Phys.* **2007**, *45*, 502.

43. Wu, S. *J. Polym. Sci. Part C* **1971**, *34*, 19.